Journal Name

ROYAL SOCIETY OF CHEMISTRY

ARTICLE

Selective hydroconversion of levulinic acid to γ-valerolactone or 2-methyltetrahydrofuran over silica-supported cobalt catalyst

Gyula Novodárszki,[a] Hanna E. Solt,[a] József Valyon,[a] Ferenc Lónyi,[a] Jenő Hancsók,[b] Dhanapati Deka,[c] Róbert Tuba[a] and Magdolna R. Mihályi *[a]

Solvent-free hydroconversion of levulinic acid (LA) was studied over Co/silica catalysts applying flow-through fixed-bed microreactor. Consecutive hydrogenation/hydrogenolysis and dehydration reactions proceeded over the catalyst having Co^0 metal and CoO_x Lewis acid active sites. As a first step, LA was dehydrated to form angelica lactone (AL) intermediate. Because dehydration of LA is a facile reaction, the selectivity was controlled by the hydrogenation/hydrogenolysis activity of the catalyst. At 200 °C and 30 bar total pressure in the steady state, the catalyst could only saturate the double bond of AL ring. Thus, γ-valerolactone (GVL) was obtained with 98 mol% yield at full LA conversion. However, at temperature ≥225 °C the hydrogenation activity was high enough to cleave the GVL ring and obtain 2-methyltetrahydrofuran (2-MTHF) with a stable yield of about 70 mol %. FT-IR spectroscopic examination of the adsorbed LA showed the formation of H-bound LA and also surface carboxylate. 4-Hydroxy-3-pentenoate and 4-hydroxypentanoate were substantiated as surface intermediates of lactone formation by dehydration.

Introduction

Due to progressive increase of global energy demand and continuous depletion of fossil carbon sources, the renewable lignocellulosic biomass attracts increased interest as source of fuel and chemicals. Lignocellulosic material is abundantly available and inexpensive, moreover it can be extensively produced and utilized without conflicting with food production. Hydrolysis of its polysaccharide components, such as cellulose and hemicellulose, gives hexoses and pentoses.

Chemocatalytic or biocatalytic processing of sugars provides us with value-added chemicals that can serve as platform compounds for the chemical industry.[1] One of these is levulinic acid.[2,3] Over the last decades, there has been an increasing interest to scale up its production (GF Biochemicals and Segetis companies) and its commercial application as chemicals (Avantium). From LA a broad spectrum of chemical products, pharmaceuticals, solvents, polymers, agricultural and energy products can be synthesized.[4–10]

In consecutive hydrogenation and dehydration steps LA can be transformed to γ-valerolactone.[11–16] Hydrogenolysis of the
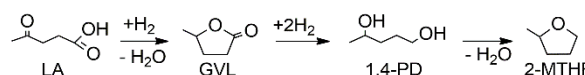
ester bond (O-(C=O)) of GVL and subsequent dehydration of the 1,4-PD intermediate gives 2-MTHF (Scheme 1).[17]

The catalyst and the reaction conditions can direct the ring opening of GVL in another pathway. The cleavage of the C-O bond on the methyl side of GVL and subsequent hydrogenation of the pentenoic acid intermediate results in pentanoic acid (PA) over bifunctional catalysts, having metal and Brønsted sites.[18] PA can further be hydrogenated to pentanols. The pentanoic acid reacting with 1-pentanol gives pentyl valerate.

GVL can be used as gasoline surrogate,[19] solvent, flavoring agent, and building block of polymers.[7] 1,4-PD may find application in the production of bio-based polymers.[7] 2-MTHF can be used as solvent.[20] It is hydrophobic, therefore it can be blended with conventional hydrocarbon fuels in high percentage.[21] Also high blend ratios of valerate esters and gasoline and diesel can be applied.[18]

This study relates to products that can be obtained by catalytic LA hydroconversion. The phrase hydroconversion covers here all the parallel and consecutive reactions that proceed if LA and hydrogen are contacted with a catalyst, including hydrogenation-dehydrogenation, hydrogenolysis, isomerization, dehydration, etc.

The efficient production of GVL from LA was demonstrated over both homogeneous and heterogeneous noble metal (mainly Ru) and non-noble metal catalysts using either

a. Institute of Materials and Environmental Chemistry, Research Centre for Natural Sciences
Hungarian Academy of Sciences
Budapest H-1117, Hungary
E-mail: mihalyi.magdolna@ttk.mta.hu
b. Institute of Chemical and Process Engineering
University of Pannonia
Veszprém H-8201, Hungary
c. Biomass Conversion Laboratory, Department of Energy
Tezpur University
Tezpur-784028, Assam, India
Electronic Supplementary Information (ESI) available: See DOI: 10.1039/x0xx00000x

Scheme 1 Hydroconversion of LA to GVL and 2-MTHF.

molecular H_2 or formic acid as hydrogen source.[11–16] The hydroconversion of LA to 2-MTHF is more challenging due to the chemical stability of the GVL intermediate. Thermodynamic calculations showed that GVL ring-opening to 1,4-PD is highly endothermic process at 250 °C (ΔG_0 = 70 kJmol^{-1}). It is energetically less favourable than the GVL ring-opening to pentenoic acid (ΔG_0 = 4 kJmol^{-1} at 250 °C) or the production of GVL from LA.[22] Thus, severe conditions (high temperature and pressure) need to get 1,4-PD from GVL. 1,4-PD should be cyclodehydrated to produce 2-MTHF. The dehydration reaction is an exothermic process (ΔG_0 = -70 kJmol^{-1} at 250 °C), which should be favoured at lower temperatures. Therefore, catalysts with well-balanced hydrogenation (metal sites) and dehydration functions (acid sites) are required to adjust the optimum rate of successive, thermodynamically unfavourable and favourable reactions so that the desired molecules should be obtained with high yield, selectivity and efficiency under milder conditions.

In an early study[23] 2-MTHF was reported as byproduct when GVL was hydrogenated to 1,4-PD over copper-chromium oxide catalyst under severe reaction conditions such as high H_2 pressure (200 bar). Recently, more efficient homogeneous and heterogeneous catalysts have been developed for 2-MTHF synthesis from LA or GVL. Ru/phosphine complexes were shown to be active and selective homogeneous catalysts in the reaction.[17] The selectivity of the complex in the conversion of LA to GVL, 1,4-PD intermediates or 2-MTHF was shown to depend on the Ru ligand and the acidity of the catalytic system.[24,25]

Using supported noble and non-noble metallic and bimetallic catalysts, it also turned out that the acid-base character of the catalyst is of significant influence on the 1,4-PD, 2-MTHF,[26-29] and alcohol selectivity.[28] The selectivity was also shown to depend on the applied H_2 pressure,[30-35] the solvent type[33,34] and the amount of the supported transition metal.[31] It is evident that water, which must accumulate during LA hydroconversion in batch reactor, suppresses dehydration and, thereby, the formation of cyclic ether.[36]

Cu and Ni are widely used in the hydroconversion of LA and GVL, however less studies concern Co-based catalysts. Unsupported cobalt catalyst prepared from commercially available Co_3O_4 was shown to be active in the hydrogenation of ethyl levulinate to GVL in batch reactor.[37] Hydrotalcite-derived Co/Al_2O_3 catalysts with high Co loading (54-85 %) were investigated in LA conversion to GVL.[38] The strong interaction between Co and Al species were shown to stabilize the Co particles against leaching and sintering. More recently, bimetallic $CuCo/Al_2O_3$ catalysts have been attempted for the hydrogenation of ethyl levulinate to 1,4-pentanediol.[39] Cobalt nanoparticles embedded in HZSM-5 zeolite crystals have found to be efficient in the conversion of LA in the presence of ethanol to pentanoic acid and ethyl pentanoate.[40] In line with earlier results,[18] we recently confirmed that the route of GVL ring opening strongly depends on the hydrogenation activity and the acidity of bifunctional heterogeneous catalysts.[41] Recently, silica-supported Co catalyst, having 20 wt% metal content have been reported to be effective in the vapour-phase hydrodeoxygenation of LA to GVL.[42] Continuous transformation

of LA to 2-MTHF over Co-based catalyst has not been reported yet.

For large-scale catalytic LA hydroconversion flow-through, continuous reactor, operating with active, selective, and stable non-noble metal heterogeneous catalyst under mild reaction conditions would be preferable.

Despite the recent significant progress achieved in developing more and more effective catalysts with improved selectivity to desirable biomass-derived products, better knowledge of the physical–chemical features of the catalyst and reaction mechanisms are needed to design efficient processes. So far, less attention has been paid to the key steps of the heterogeneous catalytic reaction, such as adsorption of the reactant onto active sites and formation and conversion of various adsorbed intermediates.

We report here about solvent-free LA conversion to GVL or to 2-MTHF over silica-supported Co catalysts with hydrogen using continuous flow, tubular, fixed-bed microreactor. The catalysts were characterized in detail before and after LA hydroconversion reaction to learn about the surface structures responsible for the catalytic activity and selectivity. Chemisorbed levulinic acid was identified on the fresh and used catalysts by FT-IR spectroscopy. Surface Co-levulinate was substantiated as the most abundant surface intermediate of the catalytic LA hydroconversion. Relationship between the formation of these species and the hydrogenation/hydrogenolysis activity of the catalyst, and thus the product distribution was studied.

It will be shown, that proper choice of the reaction conditions allows tuning the solvent-free LA hydrodeoxygenation towards the selective production of either GVL or 2-MTHF over Co/SiO_2 catalyst.

Experimental

Catalyst preparation

Catalysts of different Co contents were prepared by wet impregnation of silica (CAB-OSIL M5, Cabot Corp. Specific surface area 179 m^{2}g^{-1}, Table S1) by an aqueous solution of $Co(NO_3)_2*6H_2O$. 10 g of silica was suspended in different amounts of 0.4 M cobalt-nitrate solution. The suspensions were dried at 110 °C for 12 h. The surface-bound nitrate was decomposed by heating the sample in air at 500 °C for 3 h. The air-calcined samples contain 4.6, 8.1 and 13.3 wt% Co. Samples are designated as Co_3O_4/SiO_2 (X), where X stands for the Co content in (wt%) units. The specific surface area of the catalysts is given in Table S1. Before catalytic test the supported oxide was reduced *in situ* in the catalytic microreactor *(vide infra)* by flowing H_2 at 450 °C for 2 h. The thus reduced catalyst is referred to as $Co/SiO_2(X)$, where X stands for the Co content of the oxide precursor. The Co content of the catalyst precursor oxides was determined by atomic absorption spectroscopy (AAS).

X-ray powder diffraction (XRD)

X-ray powder diffraction patterns were recorded by Philips PW 1810/3710 diffractometer, equipped with graphite

monochromator. Radiation CuK$_\alpha$ (λ=0.1541 nm) was used. The X-ray tube was operated at 40 kV voltage and 35 mA current. The scan step size was 0.02 degrees 2-theta, whereas the scan time was five seconds in each step. *In-situ* X-ray diffraction measurements were carried out using a type HT1200 Anton Paar high-temperature sample chamber.

TEM analysis

Morphology and distribution of metal particle size on the catalysts were characterized by Transmission Electron Microscopy (TEM). Diluted suspensions of samples in water were prepared and drop-dried on carbon coated copper TEM grids. TEM images were taken by type Morgagni 268D microscope (100 kV, W filament, point-resolution= 0.5 nm).

Temperature-programmed reduction by hydrogen (H$_2$-TPR)

The reducibility of cobalt was studied by temperature-programmed reduction method (H$_2$-TPR). About 100 mg of Co$_3$O$_4$/SiO$_2$ sample was treated in a quartz reactor tube (6 mm ID) in O$_2$, flowing at a rate of 30 cm^{3}min^{-1}, at 500 °C for 1 h.

In order to obtain H$_2$-TPR curve the sample was cooled to 40 °C flushed with N$_2$ for 10 min, exposed to a 20 cm^{3}min^{-1} flow of 9.0 vol% H$_2$/N$_2$ mixture, and then heated up to 800 °C at a rate of 10°Cmin^{-1}. The reactor effluent was passed through a trap cooled by liquid nitrogen (-196 °C) to remove water from the gas flow. The rate of hydrogen uptake was followed by monitoring the H$_2$ concentration of the gas by a thermal conductivity detector (TCD) next to the trap.

X-ray photoelectron spectroscopy

XPS analyses were carried out using an electron spectrometer manufactured by OMICRON Nanotechnology GmbH. The photoelectrons were excited by non-monochromatized AlK$_\alpha$ (1486.6 eV) radiation. Spectra were recorded in the Constant Analyser Energy mode of the EA125 energy analyzer with 30 eV pass energy resulting in a spectral resolution around 1 eV. Before collecting spectra, the pellet, pressed from the air-calcined catalyst powder, was annealed in situ in vacuum at 400 °C for 1 h then cooled to room temperature. The pellet was then transferred into the preparation chamber of the spectrometer and reduced by H2 (100 mbar) at 450°C for 1 h. Charging effect was compensated by adjusting the binding energy of the Si 2p peak to 103.5 eV.[43]

Data were processed using the CasaXPS software package (N. Fairley, www.casaxps.com, 2006) by fitting the spectra with Gaussian-Lorentzian product peaks after removing a Shirley or linear background. Nominal surface compositions were calculated using the XPS MultiQuant software package[44] with the assumption of homogeneous depth distribution for all the components.

FT-IR investigations

Transmission Fourier-transform infrared (FT-IR) spectra of adsorbed species were recorded by a Nicolet Impact Type 400 spectrometer applying the self-supported wafer technique and using an in-situ cell allowing in-situ heating in gas flow or in static/dynamic vacuum. Spectra were recorded at room temperature averaging 32 scans at a resolution of 2 cm^{-1}. Spectra were normalized to wafer thickness of 5 mgcm^{-2}. Difference spectra were generated by subtracting the spectrum of the wafer from the spectrum of the wafer loaded by adsorbate. The detailed parameters are shown in the caption of the respective figures. The amount of Lewis acid sites was calculated from the integrated absorbance of the 1450 cm^{-1}-pyridine band in the spectrum obtained by degassing the wafer at 200°C after pyridine adsorption. For the calculation, the integrated molar extinction coefficient of 2.22 cmμmol^{-1} was used.[45]

Catalytic measurements

We report here about solvent-free catalytic conversion of LA over silica-supported Co-catalysts in the presence of hydrogen. The experiments were carried out in a down-stream, fixed-bed, and stainless steel tube reactor (12 mm ID). The reactor was loaded with 1 g of the 0.315-0.630 mm size sieve fraction of Co$_3$O$_4$/SiO$_2$ grains. Prior to catalytic runs the supported cobalt oxide was reduced *in-situ* in an H$_2$ flow of 100 cm^{3}min^{-1} at 30 bar and 450 °C for 2 h. Levulinic acid (98 %, Sigma Aldrich) was then fed into the reactor by high-pressure micro pump (Gilson, Model 302). The total pressure and the reaction temperature were varied in the range of 1-30 bar and 200-350 °C, respectively. The space time of LA was varied between 0.25 and 1.0 g$_{cat}$g$_{LA}^{-1}$h. The H$_2$/LA molar ratio was 12. In the present study the conditions of 200 °C, 30 bar total pressure, and 1.0 g$_{cat}$g$_{LA}^{-1}$h space time are referred to as standard reaction conditions. The reactor effluent was separated to liquid and gaseous products at room temperature. Products were analysed by GC-MS (Shimadzu QP2010 SE) using a 30 m ZB-WAX PLUS capillary column. The experimental error in all the data, provided is within typical GC errors (ca. 5–10 %). The carbon content of the feed and that of the reactor output deviated less the 5 % in each catalytic run.

Results and discussion

The preparation containing about 8 wt% Co on silica showed the best catalytic properties (*vide infra*). The characterization of this catalyst is presented below, whereas the properties of the other catalyst preparations are provided as electronic supporting information (ESI).

X-ray diffraction

Fig. 1 shows the XRD patterns of the preparation Co$_3$O$_4$/SiO$_2$(8.1). Crystalline Co$_3$O$_4$ phase was identified in the air- calcined sample (Fig. 1a). The average Co$_3$O$_4$ particle size, calculated from the Scherrer equation using the 2θ = 36.9° reflection, was about 35 nm that is in line with the result obtained by Khodakov et al.[42] for a similar preparation. This size is slightly larger than the most frequent 33 nm pore diameter of the silica support. Face-centered cubic (fcc) Co^0 lines were detected in the XRD pattern of the reduced catalyst at 2θ = 44.2
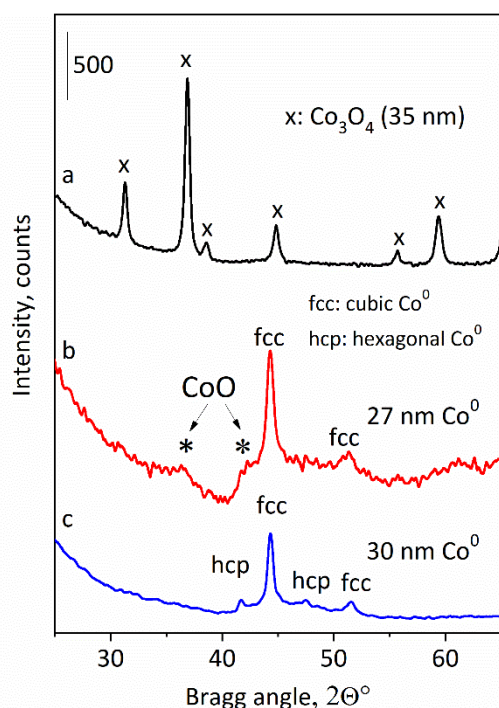
Fig. 1 XRD patterns of the Co_3O_4/SiO_2 (8.1) catalyst, (a) air-calcined at 500 °C, (b) reduced in-situ in the X-ray chamber, and (c) reduced in situ in the catalytic reactor and used for LA conversion at 200 °C for 20 h. The reductions were carried out in an H_2 flow of 50 cm³min⁻¹ at 450 °C for 1 h. The standard reaction conditions were applied. The diffractograms were recorded at room temperature.

and 51.5° (Figure 1b). The calculated average Co^0 particle size was 27 nm, in good agreement with that obtained by the H_2 chemisorption method (Table S1). The weak broad line at $2\theta = 42.4°$ comes from CoO phase, indicating that the reduced catalyst is not fully reduced (Fig. 1b). Weak lines of hexagonally close-packed (*hcp*) Co^0 in the pattern of the used catalyst show that the *fcc* structure of some Co^0 transforms to *hcp* during catalytic run (Fig. 1c).

The low-intensity broad line suggests that about 10-15 % of the cobalt remained in the sample as highly dispersed oxide. The trans-crystallization of the *fcc* cobalt to *hcp* form most probably proceeds in dissolution-recrystallization steps. The minor amount of Co found in the product mixture shows that cobalt dissolution and leaching is possible (*vide infra*). During a 20-h catalytic run under standard reaction conditions, the size of Co^0 particles remained virtually unchanged (30 nm).

In agreement with the XRD results, spherical Co particles and agglomerates with a mean diameter of 20-30 nm were observed for the reduced $Co/SiO_2(8.1)$ catalyst by TEM (Fig. S1). Homogeneous distribution of Co metallic particles was clearly seen in the TEM image of the catalyst. Note that slightly higher Co particle size (37 nm) was obtained by H_2 chemisorption (Table S1).

H_2-TPR results

The H_2-TPR curve of the $Co_3O_4/SiO_2(8.1)$ catalyst shows strongly overlapping reduction peaks in the 300-450 °C temperature range and a low-intensity broad peak in the range of 450-800 °C (Fig. 2A). Schanke et al.[43] suggests that the reduction of Co_3O_4
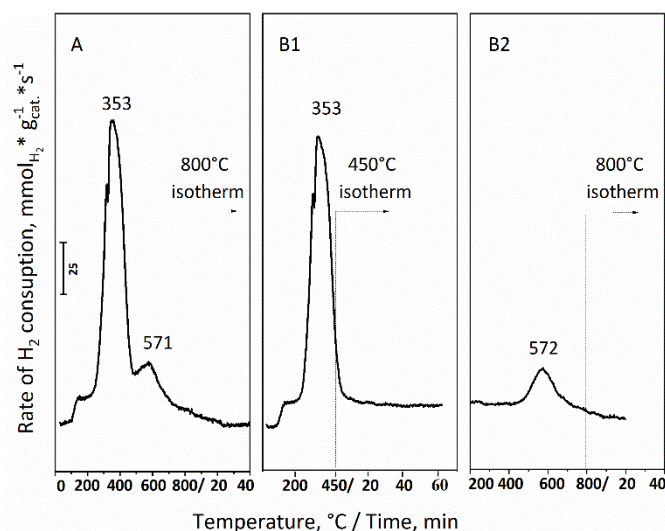

Fig. 2 H_2-TPR curves of $Co_3O_4/SiO_2(8.1)$ sample. Sample was treated in O_2, flowing at a rate of 30 cm³min⁻¹ at 500 °C for 1 h, cooled to 40 °C, flushed with N_2 then (A) heated at a rate of 10 °Cmin⁻¹ up to 800 °C in a flow of 9.0 vol% H_2/N_2 mixture. In a similar experiment (B1) temperature raising was stopped at 450 °C, sample was cooled, and (B2) the temperature was ramped up again to 800 °C.

to Co^0 is a two-step process. ($Co_3O_4 + H_2 \rightarrow 3CoO + H_2O$ and $CoO + H_2 \rightarrow Co + H_2O$). The peaks cannot represent these steps rather the distribution of oxide particle size and/or their binding strength to the silica support. The peak in the temperature range of 450-800 °C can probably be ascribed to Co species being in strong interaction with the silica support.

In line with earlier results,[44] we found that the Co_3O_4/SiO_2 sample consumed 2.59 H/Co up to 800 °C. This corresponds to a reduction degree of 97 % considering that 2.67 H/Co is needed for the total reduction of Co_3O_4 to Co^0.

Before the catalytic runs, catalysts were reduced in H_2 at 450 C for 1 h. In the TPR measurements (Fig. 2, B1 and B2) the catalyst obtained similar treatment. Results suggest that the Co-catalyst activated by pre-reduction is reduced to a degree of about 90 %. Fig. 2, B2 gives information about the cobalt, remained in cationic form. The cationic cobalt represents Lewis acid site (*vide infra*). Similar reduction degrees were observed for the other Co/SiO_2 catalyst preparations (Table S1).

CO chemisorption

The FT-IR spectra of chemisorbed CO were recorded to characterize the structure, electronic state, and environment of the sorption site (Fig. 3). No vibration band of adsorbed CO appeared in the spectrum of the sample reduced at 300 °C. Reduction to metallic cobalt particles (Co^0) begins at 350 °C that is confirmed by the appearance of the ν_{CO} band at 2006 cm⁻¹ assigned to CO linearly bound to cobalt metal.[45,46] The component band in the region of 1930-1910 cm⁻¹ suggests that bridged CO, i.e., CO bound to two Co atoms, is also present as surface species.[45] The extent of reduction and the CO uptake was higher when higher reduction temperature was applied, as indicated by the strength of the band at 2006 cm⁻¹. However, high temperature treatment can affect also cobalt dispersion that is also reflected by the absolute and relative intensities of the CO bands.
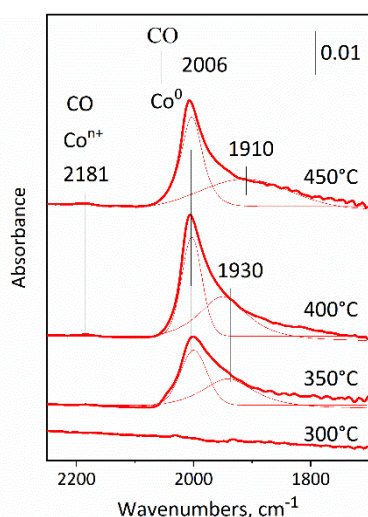
Fig. 3 FT-IR spectra of CO adsorbed on $Co_3O_4/SiO_2(8.1)$ reduced to different extents. Reduction was carried out by H_2 flow at the indicated temperature *in-situ* in the IR cell for 1 h. At each temperature, the catalyst was degassed by evacuation, cooled to room temperature, and contacted with CO at 5 mbar pressure for 10 min. After evacuation for 0.5 h, a spectrum was recorded and the temperature was increased to the next higher temperature for reduction treatment. The thin lines under the curves give the component bands obtained using a peak fitting computer program.

The surface concentration of linearly bonded CO decreased, whereas bridged CO increased, indicating a tendency for particle agglomeration at higher temperature. A weak band was also observed at 2181 cm^{-1}, which is due to the CO adsorbed on Co^{n+} (n=2,3) species.[47,48]

These results suggest that after H_2-reduction at 450 °C the majority of Co_3O_4 was reduced to Co^0, but small amount of finely dispersed CoO_x remained on the silica surface. This finding is in accordance with the XRD results. Higher amount of bridged type CO was detected on the $Co_3O_4/SiO_2(13.3)$ catalyst having about twice as large Co particles (42 nm) as the $Co_3O_4/SiO_2(8.1)$ catalyst had (Fig S2B, c and Table S1). Only very weak band of linearly bound carbonyl group was obtained from the CO adsorption over the catalyst of low Co-content (Fig. S2B, a).

XPS results

The XP spectra of the Co2p energy region are given for the air-calcined and the reduced $Co/SiO_2(8.1)$ catalyst in Fig. 4. The Co2p XP spectrum of the oxidized catalyst is identical to the spectrum of Co_3O_4.[50] The bands at the binding energy of 780-781 and 794-795 eV are due to the Co $2p_{3/2}$ and Co $2p_{1/2}$ levels of the two Co cations (Co^{2+} and Co^{3+}), respectively (Fig. 4a). Upon reduction at 450 °C by hydrogen, the XP spectrum changed significantly (Fig. 4b). The bands of ionic cobalt almost disappeared, only a weak component band remained at 780.4 eV. New peaks were observed at 778 and 793 eV, which are attributed to Co^0 $2p_{3/2}$ and Co^0 $2p_{1/2}$, respectively.

This clearly indicates the majority of surface cobalt is in metallic state in the reduced $Co/SiO_2(8.1)$ catalyst. The low intensity band at780.4 eV suggests that 5-8 % of Co remained ionic state These XPS results are in accordance with the XRD, H_2-TPR and CO chemisorption results.
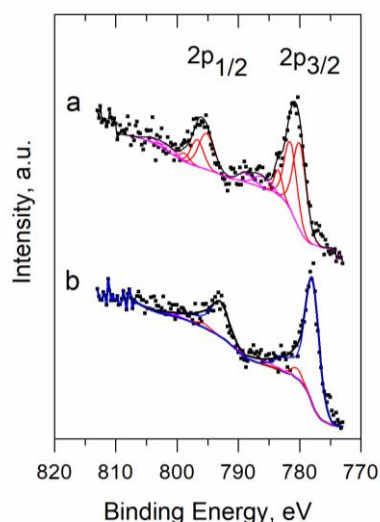

Fig. 4 XP spectra of Co 2p on (a) air-calcined and (b) reduced $Co/SiO_2(8.1)$ catalyst.

Catalyst acidity

Catalyst acidity was shown to influence the product distribution of LA and GVL hydroconversion. In homogeneous catalytic conversion the dehydration reactions could be controlled by setting the acidity of the reaction medium.[24,25] Du et al.[29] showed that the 1,4-PD or 2-MTHF selectivity of Cu/ZrO_2 catalyst in the conversion of GVL depends on the acidity of the catalyst. In absence of acid sites, the formation of 1,4-PD prevailed, whereas weak acid sites induced the intramolecular dehydration of 1,4-PD to get 2-MTHF. In presence of acidic zeolite H-Beta support dehydration of 1,4-PD to 2-MTHF was accelerated.[27] Moreover, GVL hydrogenolysis to valeric acid was suggested to proceed through protonated GVL intermediate generated by Brønsted acid sites.[18,41]

FT-IR spectra of adsorbed pyridine (Py) give information about the acidity of the sorption sites. Characteristic infrared absorption bands due to the 19b(8a) ring vibration modes of Py bound to Lewis acid sites, Brønsted acid sites, and silanols appear in the spectrum around 1450(1620), 1550(1630), and 1446(1597) cm^{-1}, respectively (Fig. 5). In line with earlier results,[49] only H-bonded Py can be detected on the activated pure silica support (bands at 1446/1597 cm^{-1}, Fig. 4, s100).

It is well documented that interaction of Py and silanol groups is weak.[50,51] Upon evacuation at 200 °C these species desorbed. Similar bands were obtained from adsorption of Py on silica-supported Co-catalysts and another pair of bands[49] at 1450/1608 cm^{-1} (Fig. 5). The bands became weaker and weaker, but did not disappear by gradually increasing the degassing temperature. Results suggest that catalyst $Co_3O_4/SiO_2(8.1)$ must contain two kinds of Py-bonding Lewis acid sites. The sites, which bound Py more strongly, are of stronger acidity. Comparison of the band intensities allows concluding that the concentration of the Lewis sites is higher in the calcined Co_3O_4/SiO_2 than in the reduced one. Moreover, the weak Py band at 1540 cm^{-1} indicates that the calcined Co-catalyst has also small amount of Brønsted acid sites. Similar spectra were detected on the other reduced catalysts (Fig. S3), the band intensity of Lewis bound
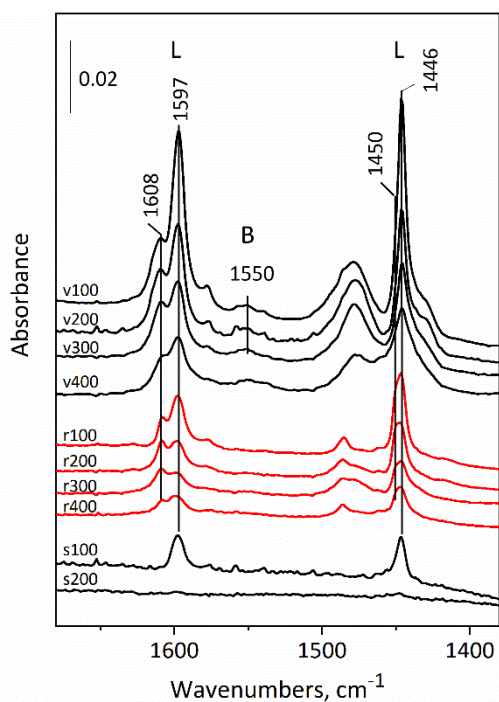
Fig. 5 FT-IR spectra of pyridine (Py) adsorbed on $Co_3O_4/SiO_2(8.1)$ catalyst activated in high vacuum at 450 °C (spectra v100-v400); reduced in H_2 flow at 450 °C (spectra r100-r400); and on the pure silica support activated in high vacuum at 450 °C (spectra s100-s200). Pre-treated samples were contacted with Py vapour at 5 mbar, 200 °C for 30 min, cooled to 100 °C and evacuated for 30 min. Evacuation was repeated at temperatures increased in 100 °C intervals. After evacuation the spectra were recorded at room temperature. Labels [L] and [B] indicate the characteristic bands for Py, bonded to Lewis- and Brønsted acid sites, respectively.

Py was proportional with the Co content. The amount of Lewis acid sites calculated from the 200°C-spectra were in the range of 14.4 and 36.9 µmolg^{-1} (Table S1).

The 1450 cm^{-1}-band has also been shown in the spectrum of the Ni/SiO$_2$ catalyst to prove that it has Lewis acidity and influences the reaction of LA to AL.[57]

Our FT-IR results evidence that the reduced Co/SiO$_2$ catalysts are strong Lewis acids, which can initiate dehydration reactions.

Hydrodeoxygenation pathways of LA

The catalytic hydrodeoxygenation of LA to GVL is believed to proceed according to Scheme 2.[52-57] On *Path I* the transformation goes through intramolecular esterification of the intermediate 4-hydroxypentanoic acid (4-HPA). On *Path II* the intermediate is α-angelica lactone (AL) formed from the enolic form of levulinic acid (5-hydroxy-γ-valerolactone, 5-HGVL) by dehydration.[53,55,56]

Abdelrahman et al.[54] showed that near to room temperature, GVL was exclusively formed through 4-HPA esterification over noble metal in aqueous phase. The carbonyl group of LA was first hydrogenated followed by acid catalyzed (Amberlyst-15) dehydrogenation. At higher temperature (265 ºC), however, AL intermediate was detected suggesting that *Path II* contributes to the LA conversion.[56] Theoretical calculations substantiated that in non-polar environment Ru catalyzed hydrodeoxygenation proceeds on active sites that are able to dissociate hydrogen homolytically and to hydrogenate the keto group of LA to get an alkoxy group that anchors activated carboxylic acid species to the catalyst surface. GVL is
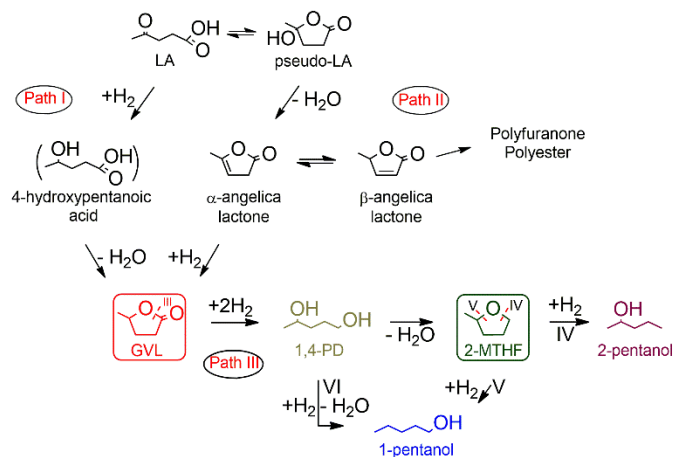
Scheme 2 Catalytic hydrodeoxygenation pathways of levulinic acid.

obtained in concerted process of ring closure and dehydroxylation of the activated surface intermediate.[58,59]

The hydrogenation activity of transition metals is lower than that of noble metals; therefore, higher temperatures are needed to activate LA for hydrodeoxygenation over Cu or Ni catalysts than over noble metal catalysts.[23,32,33] At temperatures (> 250 °C), high enough LA could be easily dehydrated to α-angelica lactone, inferring that *Path II* becomes dominant irrespective of the type of metal catalyst.[56] Temperature strongly influences the share of each reaction paths, shown in Scheme 2, in the LA hydroconversion.

It is to be noted that none of our Co/SiO$_2$ catalysts was active below 200 °C. We have studied the hydroconversion reaction and conditions varied in a reasonably broad range however, we never detected 4-HPA in the reactor effluent.

LA hydrodeoxygenation to GVL at atmospheric pressure

Intermediate AL could be identified under very specific reaction conditions only. In a series of consecutive reactions, each reaction must run with the same rate under steady state conditions. If the reaction rate constants are different then the identical rate is attained at different surface concentrations of the reactants. In the consecutive steps of LA hydrodeoxygenation AL accumulates on the catalyst surface and has a chance to appear as product if the apparent rate constant of LA dehydration is higher than the hydrogenation rate constant of the C=C bond in the AL ring.Fig. 6A shows the LA conversion as a function of space time at 250 °C. In order to decrease hydrogenation activity relative to dehydration activity we applied H$_2$ partial pressure, which is much lower than that corresponding to the standard conditions. No deactivation was detectable during the 8-hour experiment. Both AL isomers appeared in the liquid product mixture. The amount of α-AL was significantly higher than that of the β-isomer, containing conjugated double bonds. As the space time was increased the LA conversion and the yield of GVL increased. The yield of AL passed through a maximum indicating that it is intermediate of the GVL formation.

The Delplot analysis can show the rank of products.[61] In the first rank Delplot the yield-to-conversion ratio is plotted against the conversion, whereas in the second rank Delplot the selectivity-to-conversion ratio is plotted against the conversion. The
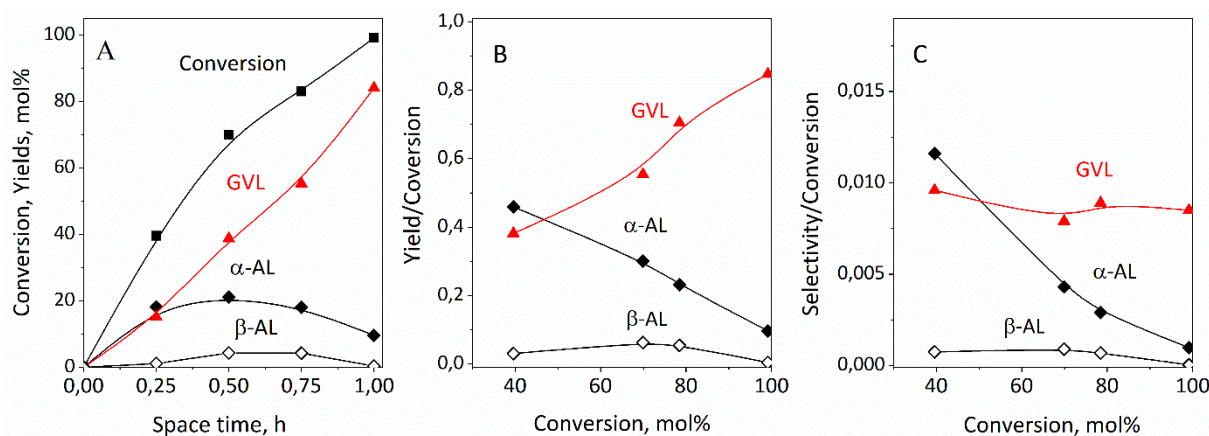
Fig. 6 LA conversion and yield of products (A) over Co/SiO2(8.1) catalyst as a function of space time at 250 °C, 1 bar total pressure, and H_2/LA ratio of 12. Responses as a function of levulinic acid conversion, first-rank delplot (B), second-rank delplot (C).

finite intercept of a line in the first-rank Delplot infers that the corresponding product is a primary product, whereas a finite intercept in a second-rank Delplot indicates that the corresponding product is a secondary product. Obviously, α-AL is primary product, whereas GVL and β-AL must be secondary products (Figs. 6B, C). Thus, LA must be first dehydrated to α-AL, which is then isomerized to the thermodynamically more stable β-form. Both ALs are then hydrogenated to GVL.

Supported Ni and Cu-based catalysts and bimetallic Cu-Ni/SiO$_2$ catalysts were reported to catalyse vapour-phase conversion of LA to GVL at atmospheric pressure in continuous flow reactor. Effect of promotor, and the role of Brønsted- and Lewis-sites were studied. Ni inhibits carbon deposition Using Ru/C, it was recently evidenced that GVL formation rate was high from aqueous LA, as water suppressed coke formation. LA hydroconversion was suggested to proceed according to a similar reaction pathway over Ni/HZSM-5 zeolite catalyst.[62] Recently, however, the transformation was substantiated to proceed simultaneously on both *Paths* at about 300 °C over Ni/HZSM-5 bifunctional catalyst.[63]

Our results suggest LA hydrodeoxygenation to GVL over silica-supported cobalt catalysts proceeds according to *Path II* of Scheme 2.

LA hydrodeoxygenation to GVL at 30 bar total pressure

Without catalyst or over pure SiO$_2$ support, under standard reaction conditions about 1 mol% LA conversion was attained and traces of α-AL, β-AL, and GVL were discerned. Similarly, low angelica lactone yields were achieved over calcined Co$_3$O$_4$/SiO$_2$(8.1) catalyst. The GVL yield was 6.6 mol% at LA conversion of 9.5 mol%. The Lewis acidity of the catalyst (cf. Fig. 5) explains dehydration activity. The hydrogenation activity is most probably due to the low amount of surface Co^0 species that could be formed in interaction with the reductive reaction mixture during the catalytic run. The hydrogenation activity of the catalyst, which was pre-reduced in situ in H$_2$ flow at 450 °C was significantly higher than that of its calcined precursor. No surprise that angelica lactone was not found in the product mixture received using reduced catalyst under standard reaction conditions, regardless of time-on-stream (TOS).

The LA conversion and the product yields are shown in Fig. 7 as a function of time-on-stream (TOS) over catalysts of different Co content at 200 °C and 30 bar total pressure. Corresponding results for the catalyst Co/SiO$_2$(4.6) are shown in Fig. S4. Full LA conversion was recorded over both catalysts from the very beginning of the experiment. Only about 3-4 % activity decrease was observed during several hours on stream. Initially high yield 2-MTHF was found. The GVL yield was initially lower but it continuously increased in time on the expense of the 2-MTHF yield. The initial 2-MTHF yield was higher on the catalyst having higher Co-content. These results suggest that GVL can be further converted in consecutive hydrogenation/hydrogenolysis/dehydration steps to 2-MTHF (Scheme 2, *Path III*).

In line with the earlier results,[24] we showed that the process is most probably introduced by the hydrogenation of the GVL carbonyl group.[41] Our quantum chemical calculations and DRIFT spectroscopic results suggested that the GVL, H-bonded through its two oxygen atoms to two hydroxyl groups of a single surface silicon atom in the vicinity of metallic Co site are the most probable activated species of the reaction. Hydrogenolysis of 2-hydroxy-5-methyltetrahydrofuran leads to 1,4-PD.[41] The 2-MTHF is the result of intramolecular 1,4-PD dehydration.

The full conversion of LA and the absence of AL in the product mixture under standard reaction conditions suggest that the process step determining the rate of consecutive reactions and product selectivity is the GVL hydrogenation/hydrogenolysis. The fresh catalyst has high hydrogenation/hydrogenolysis and dehydration activity, as suggested by the high GVL, and 2-MTHF yields, and the virtual absence of 1,4-PD in the product mixture.

The GVL and 2-MTHF yields, increasing and decreasing in time, respectively, suggests that the initially high activity of the catalyst in the hydrogenation of the carbonyl group and hydrogenolysis of the O-C bond of the GVL decreases more rapidly than the activity in the hydrogenation of the C=C bond of AL. Interestingly, the yield of 1,4-PD product passes through a maximum as a function of TOS. This could happen because the increasing surface concentration of GVL promotes the
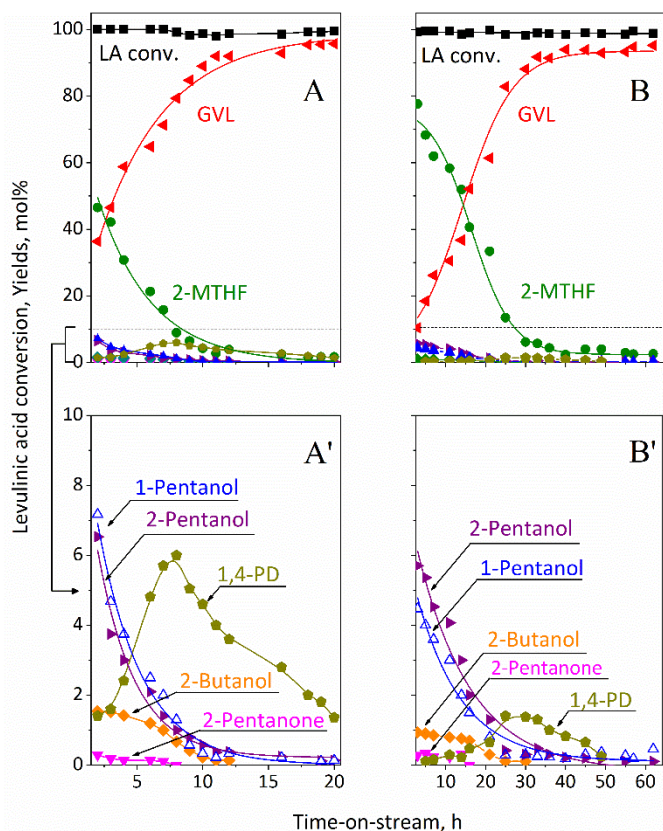
Fig. 7 LA conversion and product yields over (A, A') Co/SiO$_2$(8.1) and (B, B') Co/SiO$_2$(13.3) catalysts as a function of time on stream (TOS) at 200 °C, 30 bar total pressure, and 1.0 g$_{cat}$g$_{LA}$$^{-1}$h space time. The H$_2$/LA ratio was 12. Figures A' and B' show sections of figures A and B enlarged.

formation 1,4-PD before the drop of hydrogenolysis activity overcompensate this effect (Fig. 7).

The origin of pentanol products is a matter of discussion.[36,64] In principle both 1- and 2-pentanol can be obtained either from 1,4-PD by dehydration/hydrogenation (Scheme 2, *Path VI*) or from 2-MTHF by hydrogenolysis (Scheme 2, *Paths IV and V*). It is obvious that the prevailing route of pentanol formation is determined by the selectivity of the catalyst.

Small amount of 2-butanol was also observed. In principle, 2-butanol is possible to be formed from levulinic acid or 4-hydroxypentanoic acid by decarboxylation.[36,64,65] The other way is from 4-hydroxypentanal by decarbonylation.[36] Having hydrogenation/dehydrogenation activity it cannot be excluded that the Co/SiO$_2$ catalysts can generate 4-hydroxypentanoic acid from LA (Scheme 2, *Path I*), however, such intermediate was never detected in our study. Dehydrogenation of 1,4-PD was shown to be possible source of 4-hydroxypentanal that can be the source of 2-butanol.[36] We detected also 2-pentanone. It does not seem probable that this ketone was obtained also from the 1,4-PD. This would require a series of reactions, such as, dehydration to get 4-hydroxy-1-pentene, hydrogenation of the double bond and dehydrogenation of the obtained 2-pentanol to get 2-pentanone. An alternative explanation for the appearance of the ketone could be the spontaneous ring-opening of 2-MTHF at the C-O bond on the methyl side.[64]

The two Co-catalysts, however, showed different rates of deactivation in the GVL conversion to higher rank products like 2-MTHF. At higher Co content, the rate of deactivation was lower. When the 2-MTHF formation was virtually stopped, GVL was obtained already with selectivity higher than 95 mol% at full LA conversion. Interestingly the GVL formation continued to increase when its conversion has already stopped, suggesting that the energy barrier O-(C=O) bond hydrogenolysis is higher than the barrier of AL saturation (Scheme 2).[22]

After steady state was achieved over Co/SiO$_2$(8.1), as shown in Figure 7A the space time of LA was varied in the range of 0.25-1.0 g$_{cat}$g$_{LA}$$^{-1}$h (not shown). The initial rate of GVL formation was 5.55 μmol g$_{cat}$$^{-1}$s^{-1} at 30 bar total pressure and 250 °C, which is about 3 times greater than at 1 bar and 250 °C (calculated from Fig 6A, see Table S2). The hydrogenation reaction is supposed to proceed between the surface intermediate formed from LA or adsorbed angelica-lactone (*vide infr*a) and hydrogen adsorbed dissociatively at metallic cobalt sites. Obviously, the pressure increases the surface coverage by H atoms, thereby increasing the rate of GVL formation. The rate of GVL formation over Co/SiO$_2$(8.1) catalyst is in the range generally observed for supported non-noble metal catalysts (Table S2).

Surface species generated during LA hydroconversion

Studies often report about irreversible activity loss of heterogeneous catalysts when highly functionalized oxygenates, derived from lignocellulosic biomass, are converted in the liquid phase.[66,67] Among the possible reasons poisoning of the active sites, leaching and/or sintering of the active metal, and hydrothermal dissolution of the catalyst are mentioned. When attained steady state we stopped LA feeding and the catalyst was treated in hydrogen flow at 450 °C for 1 h (Co/SiO$_2$(8.1)). The initial activity of the catalyst was fully restored suggesting that the steady state activity of the catalyst had been developed by generation of surface species that could be relatively easily removed from the surface.
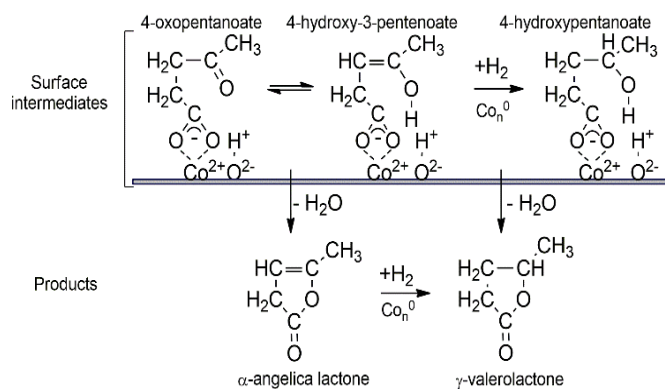
Scheme 3. Lactone formation from surface carboxylates.

Thermogravimetric examination of the used catalyst showed that the weight gain of the catalyst was 4.5 wt% until catalyst attained its steady state activity (Fig. S6).

Two species with different thermal stabilities were identified. In inert gas flow most of the surface deposit was released up to 450 °C. Two temperature ranges of weight loss were distinguished: the range below 170 °C and above up to 550 °C. No further weight loss was detected during calcination at 550 °C. The FT-IR spectroscopic examination of the used catalyst suggested that the weakly adsorbed species is H-bound LA, whereas the more strongly adsorbed species were carboxylates (*vide infra*).

Because the initial activity of the catalyst could be recovered by simply having the surface species desorbed, it seems reasonable to believe that the transitional selectivity change of the catalyst (cf. Fig. 7) was caused by the slow build-up of carboxylate species on the active surface.

While the surface carboxylate suppressed the hydrogenolysis activity of the catalyst, the dehydration and hydrogenation activity had to remain high to maintain full LA conversion.

Formation of intramolecular ester bond between an alcoholic hydroxyl and a carboxyl group to get 5-membered ring is a facile process. It seems rational to think that carboxylate forms on the silica-bound Lewis acid/Lewis base Co-cation/oxide anion pair sites and that these species are activated intermediates of intramolecular dehydration. Of course, alcoholic hydroxyl group is available only in the enol form of LA. Scheme 3 visualizes the process.

Generally, when an ester bond is formed the leaving water molecule brings the oxygen of the carboxyl hydroxide. Probably the process goes on the same way also on catalyst surface, however, direct evidence is needed.

FT-IR spectra of adsorbed reactant, reaction intermediates, and products

In order to identify the surface species formed during catalytic reaction LA was adsorbed on $Co/SiO_2(8.1)$ in presence of H_2 (Fig. 8). We investigated LA adsorption on the silica support itself.

Table 1. Vibrational frequencies and assignment for LA on SiO_2 and LA, GVL and α-AL on $Co/SiO_2(8.1)$ catalyst (ν = stretching, β = scissors bending, δ = in plane bending)

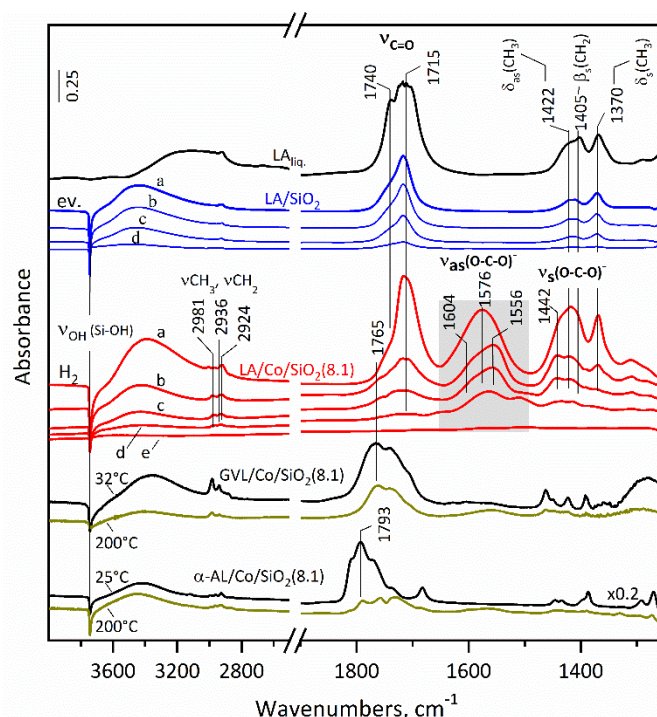| Peak position		Assignment	Comment
SiO_2	$Co/SiO_2(8.1)$		
	1793	$\nu_s(C=O)$	α-AL
	1765	$\nu_s(C=O)$	GVL
1740, 1715	1740, 1715	$\nu_s(C=O)$	carboxylic and ketone groups of H-bonded LA
	1576	$\nu_{as}(O\text{-}C\text{-}O)^{-1}$	carboxylate, LA
	1442	$\nu_s(O\text{-}C\text{-}O)^{-1}$	carboxylate, LA
1422	1422	$\delta_{as}(CH_3)$	LA
1405	1405	$\beta_s(CH_2)$	LA
1370	1370	$\delta_s(CH_3)$	LA

Fig. 8 Difference FT-IR spectra obtained from the adsorption of LA vapour on the SiO_2 support, and from the interaction of LA, GVL and α-AL with $Co/SiO_2(8.1)$ catalyst. The spectrum of LA_{liquid} was recorded using a liquid cell. The support and the catalyst were pretreated in 10% H_2/He flow of 30 $mlmin^{-1}$ at 450 °C for 1 h, evacuated at 450 °C and cooled to room temperature in dynamic vacuum. Then contacted with the vapour of the adsorptive at room temperature (i.e. 1 Pa of LA, 43 Pa of GVL or 2.53 kPa of α-AL). Spectra were recorded at room temperature after treating the pellet at temperatures, increased in successive steps. The LA/SiO_2 system was evacuated at temperatures of (a) 100 °C, (b) 200 °C, (c) 250 °C, (d) 350 °C. The $GVL/Co/SiO_2(8.1)$ and the α-$AL/Co/SiO_2(8.1)$ systems were evacuated at 200 °C. When LA was adsorbed on $Co/SiO_2(8.1)$ at 25°C, also 13,3 kPa 10% H_2/N_2 was introduced into the cell. The cell was not evacuated but the wafer was heated at temperatures (a) 100 °C, (b) 200 °C, (c) 250 °C, (d) 350 °C, (e) 450 °C.

The adsorption of reaction intermediate α-AL and GVL product were also studied on $Co/SiO_2(8.1)$ catalyst. The assignment of peaks based on literature data were summarized in Table 1.

In the spectrum of LA vapour the stretching vibration of carboxylic and keto carbonyl groups are at 1775 and 1720 cm^{-1}, respectively.[68] In the spectrum of LA liquid the corresponding bands appear redshifted to 1740 and 1715 cm^{-1} (Fig. 8), indicating that the carbonyl groups are involved in H-bonding. Adsorbed on silica the LA gives a wide band having maximum at 1715 cm^{-1}, and shoulder at about 1740 cm^{-1}. (It is to be noticed that the applied IR cell did not permit to increase the adsorption pressure of LA above its vapour pressure at room temperature. It was estimated to be as low as about 1 Pa. Informative IR spectra could be obtained only because of the high absorption coefficient of the carbonyl groups.)

The redshifts relative to the carbonyl frequencies of the LA vapour must be due to interaction of the carbonyl groups with the Si-OH groups of silica. The negative band at 3740 cm^{-1}, as well as, the intense broad shifted silanol band in the 3600-3000 cm^{-1} region indicates that silanols are involved in interaction with the LA. Most probably both carboxylic and keto carbonyls are coordinated to Si-OH groups.

The overlapping bands around 3000 cm^{-1} can be attributed to asymmetric and symmetric $\nu(CH_3)$, and $\nu(CH_2)$ stretching vibrations of methyl and methylene groups. Their deformation vibrations appear in the 1440-1350 cm^{-1} region: $\delta_{as}(CH_3)$ at 1422 cm^{-1}, $\beta_s(CH_2)$ at 1405 cm^{-1}, $\delta_s(CH_3)$ at 1370 cm^{-1}.[69] Evacuation decreased the LA coverage and the strength of its bands. All LA left the silica surface on evacuation at 350 °C.

Besides H-bound LA new surface species were obtained from the adsorption of LA on the Co/SiO$_2$(8.3) catalyst. A strong band appeared at about 1576 cm^{-1} that stems from the asymmetric stretching vibration of a carboxylate group ($\nu_{as}(COO^-)$ (Fig. 8). The band at 1442 cm^{-1}, not present in the spectrum of the silica-bound LA, most probably corresponds to the symmetric stretching vibration of COO- group ($\nu_s(COO^-)$).

The carboxylate band indicates that cobalt carboxylate must have been formed on the catalyst surface. The carboxylic group of LA became deprotonated and coordinated to cobalt cation. In principle, carboxylate could have been formed if the acid oxidized Co_n^0. Because all the carboxylate could be desorbed from the used catalyst by inert gas flushing at 450 °C, we rather believe that the carboxylate species were formed by dissociation of the carboxyl OH on the Lewis acid/Lewis base cobalt cation/oxide ion pair site (Scheme 3). In this case desorption can proceed by recombination of the carboxylate and the proton. H$_2$ was introduced into the infrared cell and the temperature of the catalyst was increased to induce reaction between H$_2$ and adsorbed LA. The carboxylate band suffered only minor erosion on temperature as high as 250 °C. This result suggests that the carboxylate species must be quite stable also at the reaction temperatures (200-225 °C) applied in the present study.

However, conditioning the catalyst pellet at 200 °C resulted in spectral changes: the maximum of the carboxylate band moved to lower wavenumbers (1556 cm^{-1}) and a shoulder became discernible at 1604 cm^{-1} (Fig. 8). This can be a sign of pentenoate/pentanoate transformation (Scheme 3) accompanied with a change of the binding geometry.[70] At higher temperature (350 °C), however, the intensity of the $\nu_{as}(COO^-)$ band significantly decreased and no adsorbed species could be detected over the catalyst treated at 450 °C. This could happen if alkanes were formed that is not detectable due to its low concentration and weak adsorption at room temperature.

The wavenumber shift of asymmetric and symmetric stretching vibration of COO$^-$ group is used for identification of the coordination type of the carboxylate group to metal cations (e.g. monodentate, bidentate chelating or bidentate bridging).[71] For Co complexes of known structure, such as Co$_2$(O$_2$CMe) complex, $\nu_{as}(COO^-)$ and $\nu_s(COO^-)$ bands appear 1565 and 1410 cm^{-1}, respectively. Such a band distance is characteristic for bridging bidentate structures. The corresponding data of a bidentate chelating Co(O$_2$CMe) complex were not available. We know only that the asymmetric stretching band appears at 1600 cm^{-1},[72] near to the 1576 cm^{-1} band that we detected. On this basis, we substantiate that the carboxylate is bound to the Co-silica catalyst as bidentate chelating complex as shown in Scheme 3.

Regarding the band assignment and thermal stability of the surface carboxylate group, our results are in accordance with the recent findings of Xu et al.,[73] who studied phthalic acid adsorption on different Co-oxides. Surface-bound carboxylates were identified and the asymmetric stretching vibration band appeared in the 1552-1548 cm^{-1} region. Phthalic acid anchored to the CoO(100) surface was shown to be stable up to 240 °C.[70] Note, that a new band is visible at 1765 cm^{-1} in the spectra of LA adsorbed on Co/SiO$_2$(8.1) at 200 and 250 °C. Such a band is most probably due to the stretching vibration of C=O of adsorbed GVL. The carbonyl band of α-angelica lactone at 1793 cm^{-1} cannot be identified in the spectra obtained from LA hydrogenation (Fig. 8).

Leaching

It is important that the catalyst support should be chemically resistant to the reactants. Leaching tests of the various supports showed that silica resisted to hot carboxylic acids,[18] such as LA and valeric acid, whereas it appears to be unstable in hot water at 200 °C.[66] When solvent-free LA reactant is hydrodeoxygenated water appears as product. Under our standard reaction conditions, at full LA conversion the partial pressure of steam was about 2 bars. In steam, the destruction of silica was not detected.

Formation surface carboxylate complex is probably the first step of metal leaching from the catalyst. With transition metals, levulinic acid was shown to form a water-soluble carboxylate complex. This explains the significant metal leaching from solid catalysts in an aqueous reaction medium.[74] One of the possible strategies of avoiding catalyst leaching is the use of ethyl levulinate as reactant. We measured the metal content of the catalysts prior to and after the catalytic run by AAS. It was found that the extent of Co leaching was dramatically affected by the level of LA conversion. When the conversion was near to complete (Fig. 7), the measured metal leaching was commensurable with the 5-8 % accuracy of the analytical method. In contrast, 12 % Co loss was measured for the catalyst Co/SiO$_2$(4.6). Latter catalyst showed high activity only for about 4 h and then the activity continuously decreased. At 20 h TOS the LA conversion was already as low as 20 mol % (Fig. S4).

Results suggest that Co leaching can be avoided if we are able to keep LA conversion near to 100 %. The catalysts of high Co-loading easily attain this, because these catalysts show high dehydration activity.

Dispersion of cobalt

It seems unlikely that the slow selectivity change would be due to decrease of Co dispersion. The metal dispersion of the fresh catalysts, determined by the hydrogen chemisorption method, was very low, i.e., 2.5 % and 1.5 % for Co/SiO$_2$(8.1) and Co/SiO$_2$(13.3), respectively (Table S1). The average size of Co crystallites prior to and after catalytic run, determined from XRD patterns (Fig. 1), was practically the same. For reduced Co/SiO$_2$(8.1) and Co/SiO$_2$(13.3) catalysts it was near to 30 nm and 40 nm size, respectively.

It is known that AL can polymerize to polyfuranone or polyester.[75] Lange et al.[18] considered AL polymerization as possible reason of catalyst deactivation. We could not identify polymers on the used catalysts suggesting that rapid hydrogenation of AL double bond suppresses polymerization at 30 bar total pressure.

Direct hydroconversion of levulinic acid to 2-MTHF

Several strategy was applied for enhancing the GVL hydrogenolysis activity of the catalysts, thus directing LA hydroconversion to the formation of 2-MTHF. By increasing the metal content[31] or applying H_2 pressure in the range of 25-70 bar[26-29,31,33-36] it could be achieved that 2-MTHF should become the main product. When the hydrogenation activity of the catalysts were high enough to open GVL ring to 1,4-PD, accelerated 1,4-PD dehydration and 2-MTHF formation could be obtained by promoting the acidic function of the catalyst.[24,25,28]

It was shown that under standard reaction conditions in the steady state GVL was virtually the only product (Fig. 7A). However, if we need 2-MTHF we have the choice to prepare it either from GVL or directly from LA. The reaction system, producing GVL, could be moved out from its steady state by simply increasing the reaction temperature. (Fig. S5). When the temperature was changed to 225 °C 2-MTHF appeared in the product mixture, indicating that catalyst gained some hydrogenation activity to further convert GVL.

However, when a fresh, pre-reduced catalyst was used at the same temperature, already 2-MTHF became the main product. The yield of 2-MTHF was about 70 mol% at 225 °C and 30 bar. The GVL yield was very low ($<$ 1 mol%), suggesting that the GVL hydrogenolysis activity was much higher than it was at 200 °C (Fig. 9). The steady state was achieved in 8 hours and the yield of 2-MTHF remained at high level in the studied 30 h period on stream. Side products, such as 2-pentanol, 1-pentanol and 2-butanol also
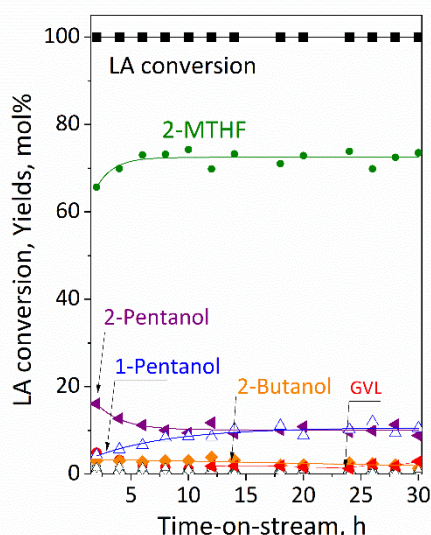
appeared. With TOS the yield of 2-pentanol decreased, whereas that of 1-pentanol increased. In steady state, virtually equivalent amount of 1-pentanol and 2-pentanol was formed at 225 °C. A higher initial yield of 2-pentanol relative to 1-pentanol suggests that 2-MTHF is preferably hydrogenated to 2-pentanol.

The catalyst was stable for up to 30 h of TOS without any deactivation.

Results show that the activity of the fresh catalyst is significantly different at 200 and 225 °C. However, the activity stabilized at 200 °C cannot be switched to the activity of the fresh catalyst at 225 °C by simply raising the reaction temperature by 25 °C.

These results show that at 200 °C the reaction generates a catalyst surface that is active and stable in the selective GVL generation from LA. However, the balance of the hydrogenation/dehydration activities responsible for the high GVL selectivity is very vulnerable. At slightly higher temperature, the increased hydrogenation activity turns GVL into intermediate of further deoxygenation reactions.

Conclusions

Co/silica catalysts, active in levulinic acid (LA) hydroconversion, were shown to contain sites of hydrogenation and dehydration activity. The most abundant surface species are Co-carboxylates formed from LA. It was substantiated that heterolytic dissociation of the acid on the Lewis acid/Lewis base pair sites of cobalt oxide gives surface levulinate anion, i.e., 4-oxopentanoate ion, and proton. Obviously, 4-hydroxy derivative was needed that ring closure should be possible by dehydration. It is generally believed that the keto carbonyl of the LA is hydrogenated prior to ring closure to lactone. Since it is more easy to hydrogenate C=C than C=O bonds it was substantiated that the enol form of the levulinate, the 4-hydroxy-3-pentenoate, is the activated species over the catalyst. The double bound is hydrogenated either before or after ring closure of the carboxylate to get γ-valerolactone.

Over catalysts, having high hydrogenation/hydrogenolysis activity GVL is further converted to 2-methyltetrahydrofuran, pentanols, pentenes and pentanes. Because dehydration of LA is a facile reaction, the selectivity of LA hydroconversion over Co/silica catalyst is controlled by the hydrogenation activity of the catalyst only. The hydrogenation activity is affected also by the carboxylate coverage of the catalyst surface. This knowledge can be applied to design more active, selective and stable non-precious metal catalysts for transformation of LA to desired products.

It was shown that using Co/SiO₂ catalyst, proper choice of the reaction conditions allows tuning the solvent-free LA hydrodeoxygenation towards the selective production of either GVL or 2-MTHF.

Conflicts of interest

There are no conflicts to declare.

Fig. 9 LA conversion and product yields over Co/SiO₂(8.1) as a function of time-on-stream (TOS) at 225 °C, 30 bar total pressure, 1.0 g$_{cat}$g$_{LA}^{-1}$h space time and H₂/LA ratio of 12.

Acknowledgements

References

1   J. J. Bozell, G. R. Petersen, *Green Chem.,* 2010, **12**, 539–554.
2   J. J. Bozell, L. Moens, D. C. Elliott, Y. Wang, G. G. Neuenscwander, S. W. Fitzpatrick, R. J. Bilski, J. L. Jarnefeld, *Resour. Conserv. Recycl.,* 2000, **28**, 227–239.
3   J. C. Serrano-Ruiz, J. A. Dumesic, *Energy Environ. Sci.,* 2011, **4**, 83–99.
4   E. I. Gürbüz, D. M. Alonso, J. Q. Bond, J. A. Dumesic, *ChemSusChem,* 2011, **4**, 357–361.
5   J. C. Serrano-Ruiz, A. Pineda, A. M. Balu, R. Luque, J. M. Campelo, A. A. Romero, J. M. Ramos-Fernández, *Catal. Today,* 2012, **195**, 162–168.
6   K. Yan, C. Jarvis, J. Gu, Y. Yan, *Renew. Sustain. Energy Rev.,* 2015, **51**, 986–997.
7   F. H. Isikgor, C. R. Becer, *Polym. Chem.,* 2015, **6**, 4497–4559.
8   C. Antonetti, D. Licursi, S. Fulignati, G. Valentini, A. Raspolli Galletti, *Catalysts,* 2016, **6**, 196-225.
9   F. D. Pileidis, M. M. Titirici, *ChemSusChem,* 2016, **9**, 562–582.
10 L. Yan, Q. Yao, Y. Fu, *Green Chem.,* 2017, **19**, 5527–5547.
11 Z. Yan, L. Lin, S. Liu, *Energy & Fuels,* 2009, **23**, 3853–3858.
12 J. Zhang, S. Wu, B. Li, H. Zhang, *ChemCatChem,* 2012, **4**, 1695–1704.
13 D. M. Alonso, S. G. Wettstein, J. A. Dumesic, *Green Chem.,* 2013, **15**, 584–595.
14 X. Tang, X. Zeng, Z. Li, L. Hu, Y. Sun, S. Liu, T. Lei, L. Lin, *Renew. Sustain. Energy Rev.,* 2014, **40**, 608–620.
15 K. Yan, Y. Yang, J. Chai, Y. Lu, *Appl. Catal. B Environ.,* 2015, **179**, 292–304.
16 F. Liguori, C. Moreno-Marrodan, P. Barbaro, *ACS Catal.,* 2015, **5**, 1882–1894.
17 H. Mehdi, V. Fábos, R. Tuba, A. Bodor, L. T. Mika, I. T. Horváth, *Top. Catal.,* 2008, **48**, 49–54
18 J. P. Lange, R. Price, P. M. Ayoub, J. Louis, L. Petrus, L. Clarke, H. Gosselink, *Angew. Chemie - Int. Ed.,* 2010, **49**, 4479–4483.
19 I. T. Horváth, H. Mehdi, V. Fábos, L. Boda, L. T. Mika, *Green Chem.,* 2008, **10**, 238–242.
20 V. Pace, P. Hoyos, L. Castoldi, P. Domínguez De María, A. R. Alcántara, *ChemSusChem,* 2012, **5**, 1369–1379.
21 M. J. Climent, A. Corma, S. Iborra, *Green Chem.,* 2014, **16**, 516–547.
22 J. C. Serrano-Ruiz, R. M. West, J. A. Dumesic, *Annu. Rev. Chem. Biomol. Eng.,* 2010, **1**, 79–100.
23 R. V. Christian, H. D. Brown, R. M. Hixon, *J. Am. Chem. Soc.,* 1947, **69**, 1961–1963.
24 F. M. A. Geilen, B. Engendahl, A. Harwardt, W. Marquardt, J. Klankermayer, W. Leitner, *Angew. Chemie - Int. Ed.,* 2010, **49**, 5510–5514.
25 A. Phanopoulos, A. J. P. White, N. J. Long, P. W. Miller, *ACS Catal.,* 2015, **5**, 2500–2512.
26 T. Mizugaki, Y. Nagatsu, K. Togo, Z. Maeno, T. Mitsudome, K. Jitsukawa, K. Kaneda, *Green Chem.,* 2015, **17**, 5136–5139.
27 T. Mizugaki, K. Togo, Z. Maeno, T. Mitsudome, K. Jitsukawa, K. Kaneda, *ACS Sustain. Chem. Eng.,* 2016, **4**, 682–685.
28 D. Licursi, C. Antonetti, S. Fulignati, M. Giannoni, A. M. Raspolli Galletti, *Catalysts,* 2018, **8**, 277.
29 X. L. Du, Q. Y. Bi, Y. M. Liu, Y. Cao, H. Y. He, K. N. Fan, *Green Chem.,* 2012, **14**, 935–939.
30 D. C. Elliott, J. G. Frye, *Hydrogenated 5-Carbon Compound and Method of Making*, 1999, US Patent 5883266.
31 P. P. Upare, J. M. Lee, Y. K. Hwang, D. W. Hwang, J. H. Lee, S. B. Halligudi, J. S. Hwang, J. S. Chang, *ChemSusChem,* 2011, **4**, 1749–1752.
32 P. P. Upare, M. G. Jeong, Y. K. Hwang, D. H. Kim, Y. D. Kim, D. W. Hwang, U. H. Lee, J. S. Chang, *Appl. Catal. A Gen.,* 2015, **491**, 127–135.
33 I. Obregõn, I. Gandarias, N. Miletic, A. Ocio, P. L. Arias, *ChemSusChem,* 2015, **8**, 3483–3488.
34 I. Obregón, I. Gandarias, M. G. Al-Shaal, C. Mevissen, P. L. Arias, R. Palkovits, *ChemSusChem,* 2016, **9**, 2488–2495.
35 G. Novodárszki, J. Valyon, Á. Illés, S. Dóbé, D. Deka, J. Hancsók, M. R. Mihályi, *React. Kinet. Mech. Catal.* 2018, DOI 10.1007/s11144-018-1507-9.
36 M. G. Al-Shaal, A. Dzierbinski, R. Palkovits, *Green Chem.,* 2014, **16**, 1358–1364.
37 H. Zhou, J. Song, H. Fan, B. Zhang, Y. Yang, J. Hu, Q. Zhu, B. Han, *Green Chem.,* 2014, **16**, 3870–3875.
38 X. Long, P. Sun, Z. Li, R. Lang, C. Xia, F. Li, *Chinese J. Catal.,* 2015, **36**, 1512–1518.
39 J. Wu, G. Gao, P. Sun, X. Long, F. Li, *ACS Catal.,* 2017, **7**, 7890–7901.
40 P. Sun, G. Gao, Z. Zhao, C. Xia, F. Li, *ACS Catal.,* 2014, **4**, 4136–4142.
41 G. Novodárszki, H. E. Solt, G. Lendvay, M. R. Mihályi, A. Vikár, F. Lónyi, J. Hancsók, J. Valyon, *Catal. Today*, 2019, 10.1016/j.cattod.2019.02.020
42 D. Sun, A. Ohkubo, K. Asami, T. Katori, Y. Yamada, *Mol. Catal.*, 2017, **437**, 105-113.
43 C. D. Wagner, A. V. Naumkin, A. Kraut-Vass, J. W. Allison, C. J. Powell, Jr. J. R. Rumble, *NIST X-ray Photoelectron Spectroscopy Database, Version 3.4,* National Institute of Standards and Technology, Gaithersburg, MD **2003**; http://srdata.nist.gov/xps/
44 M. Mohai, *Surf. Interface Anal*. 2004, **36**, 828–832.
45 C. E. Emeis, *J. Catal.,* 1993, **141**, 347-354.
46 A. Y. Khodakov, A. Griboval-Constant, R. Bechara, V. L. Zholobenko, *J. Catal.,* 2002, **206**, 230–241.
47 D. Schanke, S. Vada, E. A. Blekkan, A. M. Hilmen, A. Hoff, A. Holmen, *J. Catal.,* 1995, **156**, 85–95.
48 A. Y. Khodakov, R. Bechara, A. Griboval-Constant, *Appl. Catal. A Gen.,* 2003, **254**, 273–288.
49 K. Sato, Y. Inoue, I. Kojima, E. Miyazaki, I. Yasumori, *J. Chem. Soc. Faraday Trans. 1 Phys. Chem. Condens. Phases,* 1984, **80**, 841.
50 S. Ishi, Y. Ohno, B. Viswanathan, *Surf. Sci.,* 1985, **161**, 349–372.
51 S. Sun, N. Tsubaki, K. Fujimoto, *Appl. Catal. A Gen.,* 2000, **202**, 121–131.
52 A. Y. Khodakov, J. Lynch, D. Bazin, B. Rebours, N. Zanier, B. Moisson, P. Chaumette, *J. Catal.,* 1997, **168**, 16–25.

53 M. C. Biesinger, B. P. Payne, A. P. Grosvenor, L. W. M. Lau, A. R. Gerson, R. St. C. Smart, *Appl. Surf. Sci.* 2011, **257**, 2717-2730.

54 G. A. Mekhemer, H. M. Abd-Allah, S. A. Mansour, *Colloids Surfaces A Physicochem. Eng. Asp.,* 1999, **160**, 251–259.

55 K. Kon, W. Onodera, K. I. Shimizu, *Catal. Sci. Technol.,* 2014, **4**, 3227–3234.

56 F. Zaccheria, N. Scotti, M. Marelli, R. Psaro, N. Ravasio, *Dalt. Trans.,* 2013, **42**, 1319–1328.

57 V. V. Kumar, G. Naresh, M. Sudhakar, C. Anjaneyulu, S. K. Bhargava, J. Tardio, V. K. Reddy, A. H. Padmasri, A. Venogupal, *RSC Adv.*, 2016, **6**, 9872-9879. Lewis, atm

58 J. C. Serrano-Ruiz, D. Wang, J. A. Dumesic, *Green Chem.*, 2010, **12**, 574-577.

59 A. M. R. Galletti, C. Antonetti, V. De Luise, M. Martinelli, *Green Chem.,* 2012, **14**, 688–694.

60 O. A. Abdelrahman, A. Heyden, J. Q. Bond, *ACS Catal.,* 2014, **4**, 1171–1181.

61 W. R. H. Wright, R. Palkovits, *ChemSusChem,* 2012, **5**, 1657–1667.

62 P. P. Upare, J. M. Lee, D. W. Hwang, S. B. Halligudi, Y. K. Hwang, J. S. Chang, *J. Ind. Eng. Chem.,* 2011, **17**, 287–292.

63 J. M. Bermudez, J. A. Menéndez, A. A. Romero, E. Serrano, J. Garcia-Martinez, R. Luque, *Green Chem.,* 2013, **15**, 2786–2792.

64 O. Mamun, E. Walker, M. Faheem, J. Q. Bond, A. Heyden, *ACS Catal.,* 2017, **7**, 215–228.

65 O. Mamun, M. Saleheen, J. Q. Bond, A. Heyden, *J. Phys. Chem. C,* 2017, **121**, 18746–18761.

66 V. J. Velisoju, G. B. Peddakasu, N. Gutta, V. Boosa, M. Kandula, K. V. R. Chary, V. Akula, *J. Phys. Chem. C,* 2018, **122**, 19670-19677.

67 N. A. Bhore, M. T. Klein, K. B. Bischoff, *Ind. Eng. Chem. Res.,* 1990, **29**, 313–316.

68 V. Mohan, C. Raghavendra, C. V. Pramod, B. D. Raju and K. S. R. Rao, *RSC Adv.*, 2014, **4**, 9660-9668.

69 V. Mohan, V. Venkateshwarlu, C. V. Pramod, B. D. Raju, K. S. R. Rao, *Catal. Sci. Tecnol.*, 2014, **4**, 1253-1259. atm

70 B. Putrakumar, N. Nagaraju, V. P. Kumar, K. V. R. Chary, *Catal. Today*, 2015, **250**, 209-2017. atm

71 R. Yoshida, D. Sun, Y. Yamada, S. Sato, G. J. Hutchings, *Catal. Commun.* 2017, **97**, 79-92.atm

72 G. B. Peddakasu, V. K. Velisoju, M. Kandula, N. Gutta, K. V. R. Chary, V. Akula, *Catal. Tod*ay, 2019, **325**, 68-72.

73 M. Popova, P. Djinović, A. Ristić, H. Lazarova, G. Dražić, A. Pintar, A. M. Balu, N. Novak Tušar, *Front. Chem.,* 2018, **6**, DOI 10.3389/fchem.2018.00285.

74 A. Cho, H. Kim, A. Iino, A. Takagaki, S. Ted Oyama, *J. Catal.,* 2014, **318**, 151–161.

75 M. Grilc, B. Likozar, *Chem. Eng. J.,* 2017, **330**, 383–397.

76 J. P. Lange, *Angew. Chemie - Int. Ed.,* 2015, **54**, 13187–13197.

77 C. Hammond, *Green Chem.,* 2017, **19**, 2711–2728.

78 D. Reichert, A. Montoya, X. Liang, H. Bockhorn, B. S. Haynes, *J. Phys. Chem. A,* 2010, **114**, 12323–12329.

79 P. Larkin, in *Infrared Raman Spectrosc.*, Elsevier, 2011, pp. 1–5.

80 T. Xu, M. Schwarz, K. Werner, S. Mohr, M. Amende, J. Libuda, *Phys. Chem. Chem. Phys.,* 2016, **18**, 10419–10427.

81 G. Deacon, *Coord. Chem. Rev.,* 1980, **33**, 227–250.

82 R.T.M. Faser, *Nature,* 1964, **202**, 691-692.

83 T. Xu, M. Schwarz, K. Werner, S. Mohr, M. Amende, J. Libuda, *Chem. - A Eur. J.,* 2016, **22**, 5384–5396.

84 A. M. Hengne, C. V. Rode, *Green Chem.* **2012**, *14*, 1064-1072.

85 T. Chen, Z. Qin, Y. Qi, T. Deng, X. Ge, J. Wang, X. Hou, *Polym. Chem.,* 2011, **2**, 1190–1194.